HHS Public Access

Author manuscript

Biochim Biophys Acta Mol Basis Dis. Author manuscript; available in PMC 2024 February 10.

Published in final edited form as:

Biochim Biophys Acta Mol Basis Dis. 2022 November 01; 1868(11): 166505. doi:10.1016/j.bbadis.2022.166505.

TRPC6 N338S is a gain-of-function mutant identified in patient with doxorubicin-induced cardiotoxicity

Tong Lu[a,*], **Xiaojing Sun**[a], **Brian M. Necela**[b], **Hon-Chi Lee**[a], **Nadine Norton**[b]

[a]Department of Cardiovascular Medicine, Mayo Clinic, Rochester, MN, USA

[b]Department of Cancer Biology, Mayo Clinic, Jacksonville, FL, USA

Abstract

The canonical transient receptor potential 6 gene, *TRPC6*, has been implicated as a putative risk gene for chemotherapy-induced congestive heart failure, but knowledge of specific risk variants is lacking. Following our genome-wide association study and subsequent fine-mapping, a rare missense mutant of TRPC6 N338S, was identified in a breast cancer patient who received anthracycline-containing chemotherapy regiments and developed congestive heart failure. However, the function of N338S mutant has not been examined. Using intracellular Ca^{2+} imaging, patch clamp recording and molecular docking techniques, we assessed the function of N338S mutant heterologously expressed in HEK293 cells and HL-1 cardiac cells. We found that expression of TRPC6 N338S significantly increased intracellular Ca^{2+} levels ($[Ca^{2+}]_i$) and current densities in response to 50 μM 1-oleoyl 2-acetyl-sn-glycerol (OAG), an activator of TRPC6 channels, compared to those of TRPC6 WT. A 24-h pretreatment with 0.5 μM doxorubicin (DOX) further potentiated the OAG effects on TRPC6 N338S current densities and $[Ca^{2+}]_i$, and these effects were abolished by 1 μM BI-749327, a highly selective TRPC6 inhibitor. Moreover, DOX treatment significantly upregulated the mRNA and protein expressions of TRPC6 N338S, compared to those of TRPC6 WT. Molecular docking and dynamics simulation showed that OAG binds to the pocket constituted by the pore-helix, S5 and S6 domains of TRPC6. However, the N338S mutation strengthened the interaction with OAG, therefore stabilizing the OAG-TRPC6 N338S complex and enhancing OAG binding affinity. Our results indicate that TRPC6 N338S is a gain-of-function mutant that may contribute to DOX-induced cardiotoxicity by increasing Ca^{2+} influx and $[Ca^{2+}]_i$ in cardiomyocytes.

Keywords

TRPC6; Gain-of-function mutation; Doxorubicin; Diacylglycerol analog; Cardiotoxicity

[*]Corresponding author at: Department of Cardiovascular Medicine, Mayo Clinic, 200 First Street SW, Rochester, MN 55905, USA. lu.tong@mayo.edu (T. Lu).

CRediT authorship contribution statement

Tong Lu, Hon-Chi Lee and Nadine Norton designed the study and wrote the manuscript. Tong Lu, Xiaojing Sun, and Brian M. Necela performed experiments and analyzed the results. All authors discussed the results and commented on the manuscript.

Declaration of competing interest

The authors declare that they have no known competing financial interest or personal relationships that could have appeared to influence the works reported in this paper.

1. Introduction

Doxorubicin (DOX) is one of the most widely used anthracyclines for the treatment of adult and pediatric cancers. However, an important side effect is the cumulative, dose-related, progressive myocardial damage that may lead to heart failure. About 26 % of adult patients receiving DOX develop a significant decline in left ventricular ejection fraction (LVEF) at six months [1]. The increased risk of heart failure is observed as early as one year from the diagnosis of cancer and 7 % of patients receiving DOX develop congestive heart failure [2]. Despite guidelines for limiting the dose of DOX, there appears to be a population of patients who are vulnerable to DOX-induced cardiotoxicity. Recently, genetic studies have been used to identify genetic variants associated with chemotherapy-related heart failure with the goal of improving outcome in patients who are at high risk of therapy-induced heart failure.

According to our previous genome-wide association study (GWAS) from the NCCTG N9831 clinical trial, six novel loci were found to be associated with the maximum decline in LVEF following anthracycline-containing chemotherapy [3]. The canonical transient receptor potential 6 gene (*TRPC6*) is one of the putative risk genes [3], but fine mapping and functional validation of specific risk variants is missing. Recently, two missense *TRPC6* variant rs767086724 (p.N338S) and rs36111323 (p.A404V) were identified in cancer patients who suffered from chemotherapy-associated congestive heart failure [4]. The A404V variant was previously discovered as a gain-of-function mutant with increase in intracellular Ca^{2+} through carbachol activation in a study of familial focal segmental glomerular sclerosis (FSGS) [5] but dismissed as being causative because it is relatively common (minor allele frequency ~12 %) in the population. Our own studies of A404V in patients with heart failure who had never received DOX or trastuzumab suggest that this variant may be associated with heart failure in general [4]. The N338S variant was identified in a patient who experienced chemotherapy-induced congestive heart failure and is extremely rare in the population (minor allele frequency 0.00002 in GnomAD database). However, the pathogenic role of TRPC6 N338S mutation in cardiac function is unclear. In this study, we functionally characterized the N338S variant in HEK293 cells and HL-1 cardiac cells and tested the direct effects of DOX on the mutant channel. We found that TRPC6 N338S is a gain-of-function mutation in response to 1-oleoyl 2-acetyl-sn-glycerol (OAG), a soluble diacylglycerol analog known to directly activate TRPC6 channels [6]. OAG binds directly to the pore region of TRPC6 with a higher affinity to the N338S mutant than WT control. DOX significantly upregulated the mRNA and protein expressions of TRPC6 N338S and potentiated the channel activation to OAG.

2. Methods

2.1. Cell culture, TRPC6 mutagenesis and expression

HEK293 cells were obtained the American Type Culture Collection (ATCC) and cultured in Dulbecco's Modified Eagle medium (Sigma-Aldrich, Corp.) supplemented with 10 % fetal bovine serum and 100 μg/ml penicillin-streptomycin. HL-1 cells were kindly provided by Dr. William C. Claycomb and maintained in modified Claycomb medium (Sigma-Aldrich, Corp.) as we have previously reported [7,8]. Human TRPC6 wide type (WT) cDNA in pcDNA3.1 + C-(K)DYK was obtained

from GenScript, Inc. (clone ID: OHu23592). Mutagenesis of TRPC6 at residue N338 was carried out by substitution of asparagine (N) with serine (S), N338S, using the QuikChange Site-Directed Mutagenesis Kit (Agilent Technologies, Inc.) with the following primers: 5′-CTCGACTTCTTCAGTGCTTCTGCACAGATCAAGGAG-3′ (forward) and 5′-CTCCTTGATCTGTGCAGAAGCACTGAAGAAGTCGAG-3′ (reverse) obtained from Integrated DNA Technologies, Inc. The orientation and correctness of TRPC6 WT and TRPC6 N338S mutant were verified by DNA sequencing and their protein expression was determined by immunoblot analysis. HEK293 cells and HL-1 cardiac cells were grown on glass coverslips and then transiently co-transfected with TRPC6 WT cDNA (1 μg) or TRPC6 N338S cDNA (1 μg) together with green fluorescent protein (GFP) cDNA (0.1 μg) using Effectene Transfection Kit (Qiagen, Inc.). Forty-eight h after transfection, cells were used for patch clamp and Ca^{2+} imaging experiments.

2.2. Whole-cell patch clamp recording

Transfected cells were detected by the presence of GFP expression under an UV microscope (Olympus, IX70, Olympus America, Inc.). TRPC6 currents were evoked by a 100-ms voltage-ramp protocol from −100 mV to +100 mV preceded by a P/4 pulse condition at a holding potential of −60 mV as previously described [9,10]. The bath solution contained (in mM): NaCl 140.0, KCl 4.0, $CaCl_2$ 2.0, $MgCl_2$ 1.0, HEPES 10.0, and glucose 5.0, pH = 7.4. The pipette solution contained (in mM): Cs^+-aspartate 145.0, $MgCl_2$ 2.0, $CaCl_2$ 0.3, EGTA 10.0, and HEPES 10.0, pH = 7.35. For HL-1 cardiac cells, total cation currents were continuously recorded at baseline and application of 50 μM OAG. After the maximal effect of OAG was achieved, 1 μM BI-749327, a highly selective TRPC6 inhibitor, was superfused. The TRPC6 currents, defined as the BI-749327-sensitive components, were obtained by digitally subtracting the total currents from residual currents in the presence of BI-749327. Data were analyzed using Clampfit 10.4 software (Molecular Devices, LLC.). All experiments were performed at room temperature (24 °C).

2.3. Intracellular Ca^{2+} imaging

Intracellular Ca^{2+} concentration ($[Ca^{2+}]_i$) was measured using the fluorescence Ca^{2+} indicator, fura-2 AM (Invitrogen-Thermo Fisher Scientific, Inc.), as previously reported [10]. After a 48-h transfection with TRPC6 WT/GFP cDNA or with TRPC6 N338S/GFP cDNA, the cells were loaded with 3 μM fura-2 AM for 30 min at 37 °C. After washing with PBS or physiological saline to remove extracellular fura-2 AM, the cells were placed on the stage of an inverted Olympus IX71 microscope equipped with a Hamamatsu ORCA-R2 CCD camera (Hamamatsu Photonics, Corp.) and a Sutter LB-LS/17 light source (Sutter Instruments, Co.), and then superfused with a solution containing (in mM): NaCl 125.0, KCl 4.5, $CaCl_2$ 2.0, $MgCl_2$ 2.0, HEPES 20.0, and glucose 10.0, pH = 7.4. Intracellular Ca^{2+} fluorescence signals were measured at 510 nm from excitations of 340/380 nm. The fluorescence signals before and after application of 50 μM OAG were measured. Ca^{2+} signals (F) were analyzed using MetaFluor software (Molecular Devices, LLC.) and expressed as a ratio (F/F_0), where F_0 stands for the baseline fluorescence signal.

2.4. Surface protein biotinylation and immunoblot analysis

Surface expression of TRPC6 WT and TRPC6 N338S was determined using Surface Protein Biotinylation and Isolation Kit (Pierce Thermo Fisher, Inc.) as we have described [8]. After a 48-h transfection with TRPC6 WT or TRPC6 N338S cDNAs in HEK293 cells, the cells were washed twice with ice-cold PBS containing 1 mM $CaCl_2$ and 5 mM $MgCl_2$, incubated with PBS containing Sulfo-NHS-SS-Biotin (0.25 mg/ml) for 30 min at 4 °C, and then exposed to a quenching solution (100 mM glycine) to remove unreacted biotinylation reagent, followed by two washes with ice-cold Tris-buffered saline. Biotinylated cells were lysed with a buffer containing (in mM): NaCl 150, EDTA 1.0, Tris 20, Nonidet p-40 0.5 % (v/v) and protease inhibitor (tablet 1:25 dilution, Roche Diagnostics, Corp.), and the lysates were centrifuged at 10,000g for 10 min at 4 °C. Biotinylated proteins were incubated with 50 μl immobilized streptavidin-agarose beads for 1 h at room temperature, and the bead-bound proteins were eluted by boiling in 40 μl Laemmli buffer for immunoblot analysis.

Immunoblot analysis was performed as previously described [8]. Cytoplasmic and membrane-biotinylated proteins were separated by polyacrylamide gel electrophoresis, transferred to nitrocellulose membrane, and then immunoblotted against a mouse monoclonal anti-TRPC6 antibody (Santa Cruz biotechnology, Inc., #sc-515837). Optical densities of protein bands were analyzed using ImageJ software (JACoP, NIH). Protein expression was expressed as relative abundance normalized to GAPDH.

2.5. Quantitative real-time PCR (qRT-PCR)

Quantitative expression of TRPC6 mRNA was determined in HEK293 cells 48 h after transfection with TRPC6 WT or N338S mutant cDNAs using the iCycler iQ Real Time Detection System (Bio-Rad Laboratories, Inc.) as we have previously reported [8]. Relative cDNA replication of *TRPC6* gene was calculated according to $2^{-\Delta Ct}$ (where Ct is the cycle threshold and ΔCt = Ct of *TRPC6* gene - Ct of control gene, *GAPDH*). The reaction underwent a 40-cycle amplification with the following conditions: denaturalization for 15 s at 94 °C, annealing for 20 s at 58 °C and extension for 20 s at 70 °C. Oligonucleotide primers were synthesized by IDT Integrated DNA Technologies, Inc. and the sequences are listed as follows: TRPC6: 5′-GCCAATGAGCATCTGGAAAT-3′ (forward) and 5′-GCTGGTTGCTAACCTCTTGC-3′ (reverse); GAPDH: 5′-TGCCAAGGCTGTGGGCAAGG-3′ (forward) and 5′-TGGGCCCTCAGATGCCTGCT-3′ (reverse).

2.6. In silico methods

The 3D-structure of TRPC6 WT (PDB ID: 6UZ8) was obtained from protein database [6] and the TRPC6 N338S mutant was generated using the programs of PyMOL v1.5.0.2 (Schrödinger, LLC.). The 2D-structure of OAG (CID: #6504449) was downloaded from PubChem database, included with Gasteiger partial charges and converted in PDBQT format using the OpenBasel tool v2.3.2 [11]. Molecular docking was performed using AutoDockTools v1.5.7 (Molecular Graphics Laboratory) [12], analyzed by Protein Ligand Interaction Profiler web tool [13] and virtualized by PyMOL and VMD software [14]. To

compare the stability and conformational changes of docking pose, molecular dynamics simulation of 1 ns was carried out using the VMD graphical interface to NAMD software.

2.7. Chemicals

BI-749327 was purchased from MedChemExpress, LLC. Unless otherwise mentioned, all chemicals were purchased from Sigma-Aldrich, Corp.

2.8. Statistical analysis

Data were expressed as mean ± standard error (S.E.M). One-way ANOVA followed by Tukey's test analysis was conducted to compare multiple groups. A paired *t*-test was used to compare the mean value before and after treatment of OAG in HL-1 cells. Statistical analysis was conducted using SigmaPlot 12.0 software (Systat Software, Inc.). Statistically significant difference was defined as $p < 0.05$.

3. Results

3.1. Effect of OAG on intracellular Ca^{2+} levels in HEK293 cells expressing TRPC6 WT and N338S mutant

We measured $[Ca^{2+}]_i$ in HEK293 cells 48-h after expression of TRPC6 WT or N338S before and after superfusion with 50 μM OAG. In cells expressing TRPC6 WT, the peak F/F_0 value was increased from 1.05 ± 0.08 at baseline to 2.05 ± 0.34 with OAG ($p < 0.05$, n = 12). In cells expressing TRPC6 N338S, the peak F/F_0 at baseline was similar to that of TRPC6 WT (1.09 ± 0.05, n = 14, p = N.S. vs. WT) but had a significantly greater increase upon OAG exposure (4.31 ± 0.51, n = 14, $p < 0.05$ vs. WT) (Fig. 1A).

The effects of DOX on $[Ca^{2+}]_i$ in HEK293 cells were determined in cells after a 24-h expression of TRPC6 WT or N338S, followed by adding 0.5 μM DOX into the cell culture medium for an additional 24 h incubation. As shown in Fig. 1B, DOX treatment significantly increased $[Ca^{2+}]_i$ levels at baseline in cells expressing TRPC6 WT (F/F_0 = 1.77 ± 0.10, n = 12) or N338S (1.69 ± 0.12, n = 10), compared to cells incubated with vehicle ($p < 0.001$ for both WT and N338S). However, DOX did not change the baseline $[Ca^{2+}]_i$ levels in cells between TRPC6 WT and N338S expression, but greatly enhanced the effects of OAG on $[Ca^{2+}]_i$ in cells expressing TRPC6 N338S (F/F_0 = 2.53 ± 0.38 of WT, n = 12, vs. 6.77 ± 2.0 of N338S, n = 10, $p < 0.001$). In addition, the effects of OAG were abolished by a 30-min preincubation with 1 μM BI-749327. These results suggest that the enhanced $[Ca^{2+}]_i$ in HEK293 cells by OAG is mediated through TRPC6 channel activation, and that N338S mutant has a significant increase in $[Ca^{2+}]_i$ upon OAG with potentiation by DOX.

3.2. Effects of OAG on TRPC6 WT and N338S mutant channel currents

Fig. 2A shows representative tracings of TRPC6 WT and TRPC6 N338S currents elicited from HEK293 cells 48 h after transfection with and without exposure to 50 μM OAG. At baseline, TRPC6 N338S displayed higher inward and outward current densities compared to TRPC6 WT. A 1-hour incubation with 50 μM OAG markedly increased the inward and outward current densities of TRPC6 WT, but the effects of OAG were much greater in TRPC6 N338S. Pretreatment with DOX (0.5 μM, 24 h) significantly enhanced the baseline

inward and outward current densities of TRPC6 WT and the effects were more pronounced in TRPC6 N338S (Fig. 2B). Moreover, in cells pre-incubated with DOX, application of 50 μM OAG further augmented the inward and outward current densities of TRPC6 WT, but with significantly greater effects in TRPC6 N338S (Fig. 2C). Group results of the inward and outward current densities from TRPC6 WT and N338S channels at baseline and on exposure to OAG are summarized in Scatter dot plots.

We measured TRCP6 WT and N338S current densities in HL-1 cardiac cells 48-h after transfection with TRCP6 WT and N338S mutant cDNAs. Total cation currents were continuously recorded from HL-1 cells at baseline and on exposure to 50 μM OAG followed by 1 μM BI-749327. In cells with TRPC6 WT transfection, the inward and outward components of BI-749327-sensitive current densities were significantly increased after superfusion of 50 μM OAG. However, in cells with TRPC6 N338S transfection, there was a more marked increase in the BI-749327-sensitive current densities at baseline and on exposure to 50 μM OAG (Fig. 3A). Furthermore, a 24-h treatment with 0.5 μM DOX robustly augmented the BI-749327-sensitive current densities in cell with TRPC6 WT transfection at baseline and with application of OAG, compared to cells without DOX treatment. However, after preincubation with DOX, cells transfected with TRPC6 N338S had a much greater OAG-induced increment in the BI-749327-sensitive current densities compared to WT control (Fig. 3B). Group results with statistical difference are shown in Scatter dot plots.

3.3. Upregulation of the mRNA and protein expression of TRPC6 N338S by DOX

We measured the mRNA expression levels of TRPC6 WT and N338S in HEK293 cells 24 h after transfection with the same amount of the respective cDNAs, followed by an additional 24 h of incubation with 0.5 μM DOX or vehicle (DMSO). The levels of mRNA expression for TRPC6 WT and N338S (relative to GAPDH) were similar in cells with DMSO control, but were significantly increased with DOX treatment by 4.27 folds in cells transfected with TRPC6 WT (from 3.86 ± 0.11 with DMSO to 16.48 ± 1.19 with DOX, $n = 3$, $p < 0.001$) and by 9.02 folds in cells transfected with N338S (from 3.49 ± 0.16 with DMSO to 31.46 ± 1.58 with DOX, $n = 3$, $p < 0.001$) (Fig. 4B). To further determine these changes, we found that the surface biotinylated proteins and cytoplasmic proteins as well as the ratio of their expression between TRPC6 WT and N338S were no different in cells without DOX treatment ($n = 5$, p = N.S.). Whereas the surface biotinylated and cytoplasmic protein levels of TRPC6 N338S were significantly upregulated ($n = 4$, $p < 0.05$) without altering the ratio of their expression in cells with DOX treatment (Fig. 4C).

3.4. Homology modeling of human TRPC6 N338S

To better understand the effects of the N338S mutation on human TRPC6 structure, we compared conformational changes in the 3D-structures of TRPC6 WT and N338S mutant. Fig. 5A illustrates that functional TRPC6 protein is composed of 4 homologous subunits. In each subunit, the polar residue N338 is located at the beginning of linker helix (LH6) in the cytoplasmic N-terminus (Fig. 5B). The N338 interacts with several adjacent residues, with E340 via hydrophobic interaction (3.9 Å), with E341 via both hydrophobic (4.1 Å) and polar interactions (3.1 Å), with V342 via a hydrogen bond (3.6 Å) and polar interaction (3.3 Å).

Moreover, the N338 interacts with S268 in the linker helix 2 (LH2) of an adjacent subunit through a polar interaction (3.5 Å). Additionally, the E341 forms electrostatic interactions with R861 (2.8 Å) and R865 (2.1 Å and 2.9 Å) in the horizontal helix (HH) of the same subunit (Fig. 6A). The N338S mutation alters the interaction and distance between S338 and its adjacent residues: with E340 (via two polar bonds, 3.1 Å and 2.9 Å), with E341 (via two polar bonds, 3.3 Å and 2.9 Å) and with V342 (via a hydrogen bond, 3.6 Å and a polar bond, 3.3 Å), and adds an additional polar bond (3.6 Å) between E340 and R681 at HH within the same subunit. However, the N338S mutation interrupts its interaction with S268 in LH2 of the adjacent subunit (Fig. 6B). In summary, the N338S mutation strengthens the interactions between LH6 and HH within the same subunit but weakens the interaction of LH6 and LH2 between two adjacent subunits.

3.5. Molecular docking and dynamics simulation analysis of OAG and TRPC6 interaction

To analyze the alterations of N338S mutant on OAG-TRPC6 interaction, we performed molecular docking of OAG on TRPC6 WT and N338S proteins. OAG binds to a pocket constituted by the pore helix, S5 and S6 domains in the same subunit. Specifically, the acetyloxy group of OAG and L719 in S6 of TRPC6 WT participated in a polar interaction. The oleoyl glycerol chain of OAG formed multiple hydrophobic and polar interactions with F641, I642, and F645 in S5, and with F675 and I682 in the pore helix of TRPC6 WT (Fig. 7A). For the N338S, there were similar interactions between OAG and TRPC6 except with shorter distances. An additional residue M715 in S6 interacted with the acetyloxy group of OAG via a hydrogen bond and a polar bond. Furthermore, the connection of OAG with F675 in the pore helix of TRPC6 WT was substituted by V646 in the S5 of N338S (Fig. 7B). Such conformational changes would lead to a closer interface between OAG and N338S, supported by the result of a reduction in the binding energy of OAG (−13.97 kcal/M of N338S vs. −13.09 kcal/M of WT) and the apparent dissociation rate constant (Kd) of OAG (77.71 pM of N338S vs. 252.65 pM of TRPC6 WT). Detail molecular docking parameters are listed in Table 1. Moreover, to further confirm the structural stability of the protein-ligand docking complexes, a typical molecular dynamics simulation of 1-ns duration was carried out for OAG-TRPC6 WT and OAG-TRPC6 N338S docking poses. Root Mean Square Deviation (RMSD) was 2.22 ± 0.68 Å for OAG-TRPC6 WT and 1.92 ± 0.37 Å for OAG-TRPC6 N338S, articulating that both docking poses were stable with less conformational changes on the OAG-TRPC6 N338S complex during simulation.

4. Discussion

TRPC6 is normally expressed in cardiomyocytes at very low levels and is known to be directly activated by diacylglycerol [15,16]. Activation of TRPC6 promotes Ca^{2+} influx, elevates $[Ca^{2+}]_i$, and triggers Ca^{2+}-dependent signaling cascades [15,16]. TRPC6 channel function has been linked to cardiac physiology and pathophysiology [17]. Indeed, increased TRPC6 expression levels were observed in cardiac hypertrophy and heart failure in animal studies [18,19]. Overexpression of *Trpc6* gene enhanced the cardiac sensitivity to pressure overload and caused fatal cardiomyopathy and heart failure in cardiac-specific *Trpc6* transgenic mice [19], while genetic deletion of *Trpc6* prevents pressure-overloaded cardiac hypertrophy in mice [20,21]. Furthermore, genetic knock out of *Trpc6* significantly

improved cardiac function and survival in male mice with DOX treatment [22]. We have recently reported that *TRPC6* is a putative risk gene for chemotherapy-related decline in LVEF and congestive heart failure respectively in patients who received antineoplastic drugs [3,4]. A rare *TRPC6* variant rs767086724 (p. N338S) was identified in a 32-year-old African American woman diagnosed with breast cancer and hypertension, who completed an anthracycline-containing chemotherapy regiment (3 months of DOX, followed by 3 months of paclitaxel then 12 months of trastuzumab) [4]. Her LVEF declined from 60 % to 27.5 % after completion of therapy but recovered to 63 % after a 1.5-year followup, indicating an intimate correlation between cardiac function and chemotherapy.

In this study, we examined the function of TRPC6 N338S mutant in a heterologous expression system and in native cardiac myocytes. Our results showed that the current densities and $[Ca^{2+}]_i$ levels in cells expressing TRPC6 N338S were markedly increased upon OAG activation, compared with cells expressing TRPC6 WT. The OAG-mediated elevation of $[Ca^{2+}]_i$ was abrogated by a highly selective TRPC inhibitor BI-749327, elucidating that the increase in $[Ca^{2+}]_i$ was mediated through TRPC6 channels. Moreover, the OAG effects were augmented by a 24-h incubation with DOX. These results are confirmed by patch clamp studies, showing that TRPC6 N338S channels had significantly greater inward and outward current densities at baseline and become greatly potentiated by OAG activation as compared to WT channels. Treatment with DOX further enhanced N338S mutant channel activation to OAG. It is well-known that DOX-induced cardiotoxicity is attributed to altered Ca^{2+} handling in cardiomyocytes by multiple mechanisms, including increased Ca^{2+} influx and reduced sarcoplasmic reticulum Ca^{2+} uptake [23]. As a major factor causing Ca^{2+} entry in cardiomyocytes, TRPC6 function is modulated by reactive oxygen species (ROS) generation and protein phosphorylation [24]. For instance, TRPC6 protein phosphorylation by Src-family tyrosine kinases (Src-TK) and Ca^{2+}/calmodulin-dependent protein kinase II (CaM kinase II) provokes TRPC6 channel activity [25,26], while that by protein kinase C (PKC) and protein kinase G (PKG) suppresses TRPC6 channel function [27,28]. Since DOX promotes ROS production [29], upregulates the signaling pathways of Src kinase and CaM kinase II [30–32], and downregulates those of PKC and PKG [33–36], it is not surprising that the presence of DOX would potentiate the OAG effects on TRPC6 and induce $[Ca^{2+}]_i$ overload, particularly in cells with the gain-of-function TRPC6 N338S mutant expression.

The pathological roles of TRPC6 mutations were first discovered as a cause of familial FSGS in 2005 [37]. To date, a total of 21 different missense/frameshift variants of *TRPC6* have been implicated in familial FSGS and most of these are associated with gain-of-function except one causing childhood-onset due to the loss of TRPC6 function [5]. These gain-of-function mutations are clustered into two major regions of TRPC6. The first cluster is at the interface between ankyrin repeats (ARs), and the vertical helix (VH) and the second cluster is close to the horizontal helix (HH) [38–42]. However, the biophysical mechanism underlying gain-of-function mutation of TRPC6 is currently unclear [6]. Azumaya et al. reported that ARs and the linker helices (LHs) form a “dome-like chamber” at the C-termini of TRPC6 channels, where hydroxyl group amino acids are enriched in the inner of “dome-like chamber” that may promote cations exit from the channel [42]. Such features of TRPC6 structure may explain the cause of channel functional changes due to mutations in these

locations. According to the 3D-structure of the human TRPC6, the polar residue N338 is located at the beginning of LH6, interfacing with the distal end of HH within the same subunit. Meanwhile, the N338 directly interacts with S268 in LH2 of an adjacent subunit. Although N338 does not interact with any residues in HH, it connects to a neighboring residue E341 that forms three electrostatic interactions with R861 and 865 at HH in the same subunit (Fig 6A). Interestingly, the N338S mutation abolishes a polar interaction with S268 in LH2 of an adjacent subunit but confers an additional electrostatic interaction between E340 and R861 at HH within the same subunit (Fig. 6B). Importantly, the N338S mutation not only alters the connections to E340 and E341 by the substitution of two hydrophobic bonds with two polar bonds, but also adds two additional polar interactions to E340 and E341 (Fig. 6B). Such alterations will strengthen the connections between LH6 and HH domains in the same subunit but loosen the interaction of LH6 and LH2 domains between two adjacent subunits, which may affect the conformation of TRPC6 “dome-like chamber”.

It has been shown that the pore helix and S6 domains are critical for OAG-mediated TRPC6 channel activation [6]. Consistent with this report, we have also found that the acetyloxy group and the oleoyl glycerol chain of OAG bind to the groove composed of the pore helix, S5 and S6 domains of TRPC6 WT and N338S mutant (Fig. 7A and B). Molecular dynamics simulation confirmed the docking results, showing a high stability of these protein-ligand docking poses. Interestingly, the N338S mutant basically contains the same OAG-binding sites with TRPC6 WT except 1) shortening of the interfacial distances between OAG and N338S; 2) interacting with two additional residues, V646 in S5 and M715 in S6, through additional hydrogen and polar bonds (Fig. 7B). As a result of these changes in the OAG-N338S docking pose, showing reduced the binding energy and the apparent Kd of OAG to N338S protein, there is most likely an increase of OAG binding affinity with enhanced efficiency and efficacy of the OAG effects on N338S mutant. Thus, combining patch-clamp techniques, molecular docking and simulation analysis will further provide insights into the structural and functional basis of gain-of-function *TRPC6* variants. Notably, it should be remembered that in this study the apparent Kd of OAG-TRPC6 interaction was obtained by in silico modeling, the real Kd value should be measured directly.

Some gain-of-function TRPC6 mutants, such as K874X, R895C and E897K, exhibit an increase of their surface expression via mechanisms involving ROS signaling and the calcineurin/nuclear factor of activated T-lymphocytes (NFAT) pathway activation [24,40]. This is not the case for N338S mutant because the mRNA and protein expression levels of TRPC6 WT and N338S mutant were unchanged in cells unless treated with DOX. Previous studies have demonstrated that DOX activates ROS and calcineurin/NFAT signaling pathways in cardiomyocytes [29,43,44]. Importantly, we found that DOX exposure increased the levels of TRPC6 N338S transcription, twice as much as TRPC6 WT. However, the precise mechanism leading to enhanced N338S response to DOX stimulation warrants further investigation. Nevertheless, upregulation of the N338S surface expression by DOX provides an additional mechanism for DOX-induced cardiotoxicity.

5. Conclusion

We have provided compelling evidence that TRPC6 N338S is a gain-of-function mutation leading to increasing Ca^{2+} influx and elevating $[Ca^{2+}]_i$ in cells after OAG and DOX treatment. The TRPC6 N338S mutation has a higher binding affinity for OAG and the OAG effects are greatly potentiated by DOX in TRPC6 N338S. Importantly, the mRNA and protein levels of TRPC6 N338S are markedly upregulated in the presence of DOX. Since an increase of TRPC6 activity is intimately related to cardiomyopathy, assessment of TRPC6 function should be considered to predict and prevent anthracycline cardiotoxicity in patients carrying *TRPC6* risk variants.

Acknowledgements

This work is supported by funding from U.S. Department of Defense (W81XWH2210288) and the Department of Cardiovascular Medicine, Mayo Clinic.

Data availability

Data will be made available on request.

Abbreviations:

AR	ankyrin repeat
DOX	doxorubicin
FSGS	focal segmental glomerular sclerosis
GWAS	genome-wide association study
ICD	intracellular cytoplasmic domain
HH	horizontal helix
LH	linker helix
LVEF	left ventricular ejection fraction
NFAT	the nuclear factor of activated T-lymphocytes
OAG	1-oleoyl 2-acetyl-sn-glycerol
RMSD	root mean square deviation
ROS	reactive oxygen species
TMD	transmembrane domain
TRP	transient receptor potential
TRPC6	canonical transient receptor potential 6
VH	vertical helix

References

[1]. Drafts BC, Twomley KM, D'Agostino R Jr., Lawrence J, Avis N, Ellis LR, Thohan V, Jordan J, Melin SA, Torti FM, Little WC, Hamilton CA, Hundley WG, Low to moderate dose anthracydine-based chemotherapy is associated with early noninvasive imaging evidence of subclinical cardiovascular disease, JACG Cardiovasc. Imaging 6 (2013) 877–885.

[2]. Larsen CM, Villarraga HR, Begna KH, Litzow MR, Al-Kali A, Herrmann J, Cardiovascular effects of the addition of nilotinib to standard therapy for acute myeloid leukemia, Leuk Lymphoma 59 (2018) 229–232. [PubMed: 28592197]

[3]. Serie DJ, Crook JE, Necela BM, Dockter TJ, Wang X, Asmann YW, Fairweather D, Bruno KA, Colon-Otero G, Perez EA, Thompson EA, Norton N, Genome-wide association study of cardiotoxicity in the NCCTG N9831 (Alliance) adjuvant trastuzumab trial, Pharmacogenet. Genomics 27 (2017) 378–385. [PubMed: 28763429]

[4]. Norton N, Crook JE, Wang L, Olson JE, Kachergus JM, Serie DJ, Necela BM, Borgman PG, Advani PP, Ray JC, Landolfo C, Di Florio DN, Hill AR, Bruno KA, Fairweather D, Association of genetic variants at TRPC6 with chemotherapy-related heart failure, Front. Cardiovasc. Med 7 (2020) 142. [PubMed: 32903434]

[5]. Riehle M, Buscher AK, Gohlke BO, Kassmann M, Kolatsi-Joannou M, Brasen JH, Nagel M, Becker JU, Winyard P, Hoyer PF, Preissner R, Krautwurst D, Gollasch M, Weber S, Harteneck C, TRPC6 G757D loss-of-function mutation associates with FSGS, J. Am. Soc. Nephrol 27 (2016) 2771–2783. [PubMed: 26892346]

[6]. Bai Y, Yu X, Chen H, Horne D, White R, Wu X, Lee P, Gu Y, Ghimire-Rijal S, Lin DC, Huang X, Structural basis for pharmacological modulation of the TRPC6 channel, elife 9 (2020).

[7]. Ling TY, Wang XL, Chai Q, Lu T, Stulak JM, Joyce LD, Daly RC, Greason KL, Wu LQ, Shen WK, Cha YM, Lee HC, Regulation of cardiac CACNB2 by microRNA-499: potential role in atrial fibrillation, BBA Clin. 7 (2017) 78–84. [PubMed: 28239561]

[8]. Qian LL, Sun X, Yang J, Wang XL, Ackerman MJ, Wang RX, Xu X, Lee HC, Lu T, Changes in ion channel expression and function associated with cardiac arrhythmogenic remodeling by Sorbs2, Biochim. Biophys. Acta Mol. Basis Dis 1867 (2021), 166247. [PubMed: 34487812]

[9]. Estacion M, Sinkins WG, Jones SW, Applegate MA, Schilling WP, Human TRPC6 expressed in HEK 293 cells forms non-selective cation channels with limited Ca2+ permeability, J. Physiol 572 (2006) 359–377. [PubMed: 16439426]

[10]. Lu T, Wang XL, Chai Q, Sun X, Sieck GC, Katusic ZS, Lee HC, Role of the endothelial caveolae microdomain in shear stress-mediated coronary vasorelaxation, J. Biol. Chem 292 (2017) 19013–19023. [PubMed: 28924052]

[11]. O'Boyle NM, Banck M, James CA, Morley C, Vandermeersch T, Hutchison GR, Open babel: an open chemical toolbox, J. Cheminform 3 (2011) 33. [PubMed: 21982300]

[12]. Seeliger D, de Groot BL, Ligand docking and binding site analysis with PyMOL and Autodock/Vina, J. Comput. Aided Mol. Des 24 (2010) 417–422. [PubMed: 20401516]

[13]. Salentin S, Schreiber S, Haupt VJ, Adasme MF, Schroeder M, PLIP: fully automated protein-ligand interaction profiler, Nucleic Acids Res. 43 (2015) W443–W447. [PubMed: 25873628]

[14]. Lu T, Hong MP, Lee HC, Molecular determinants of cardiac K(ATP) channel activation by epoxyeicosatrienoic acids, J. Biol. Chem 280 (2005) 19097–19104. [PubMed: 15760904]

[15]. Wang H, Cheng X, Tian J, Xiao Y, Tian T, Xu F, Hong X, Zhu MX, TRPC channels: structure, function, regulation and recent advances in small molecular probes, Pharmacol. Ther 209 (2020), 107497. [PubMed: 32004513]

[16]. Eder P, Molkentin JD, TRPC channels as effectors of cardiac hypertrophy, Circ. Res 108 (2011) 265–272. [PubMed: 21252153]

[17]. Yamaguchi Y, Iribe G, Nishida M, Naruse K, Role of TRPC3 and TRPC6 channels in the myocardial response to stretch: linking physiology and pathophysiology, Prog. Biophys. Mol. Biol 130 (2017) 264–272. [PubMed: 28645743]

[18]. Wu X, Eder P, Chang B, Molkentin JD, TRPC channels are necessary mediators of pathologic cardiac hypertrophy, Proc. Natl. Acad. Sci. U. S. A 107 (2010) 7000–7005. [PubMed: 20351294]

[19]. Kuwahara K, Wang Y, McAnally J, Richardson JA, Bassel-Duby R, Hill JA, Olson EN, TRPC6 fulfills a calcineurin signaling circuit during pathologic cardiac remodeling, J. Clin. Invest 116 (2006) 3114–3126. [PubMed: 17099778]

[20]. Xie J, Cha SK, An SW, Kuro OM, Birnbaumer L, Huang CL, Cardioprotection by Klotho through downregulation of TRPC6 channels in the mouse heart, Nat. Commun 3 (2012) 1238. [PubMed: 23212367]

[21]. Seo K, Rainer PP, Shalkey Hahn V, Lee DI, Jo SH, Andersen A, Liu T, Xu X, Willette RN, Lepore JJ, Marino JP Jr., Birnbaumer L, Schnackenberg CG, Kass DA, Combined TRPC3 and TRPC6 blockade by selective small-molecule or genetic deletion inhibits pathological cardiac hypertrophy, Proc. Natl. Acad. Sci. U. S. A Ill (2014) 1551–1556.

[22]. Norton N, Bruno KA, Di Florio DN, Whelan ER, Hill AR, Morales-Lara AC, Mease AA, Sousou JM, Malavet JA, Dorn LE, Salomon GR, Macomb LP, Khatib S, Anastasiadis ZP, Necela BM, McGuire MM, Giresi PG, Kotha A, Beetler DJ, Weil RM, Landolfo CK, Fairweather D, Trpc6 promotes doxorubicin-induced cardiomyopathy in male mice with pleiotropic differences between males and females, Front. Cardiovasc. Med 8 (2021), 757784. [PubMed: 35096991]

[23]. Wenningmann N, Knapp M, Ande A, Vaidya TR, Ait-Oudhia S, Insights into doxorubicin-induced cardiotoxicity: molecular mechanisms, preventive strategies, and early monitoring, Mol. Pharmacol 96 (2019) 219–232. [PubMed: 31164387]

[24]. Dryer SE, Roshanravan H, Kim EY, TRPC channels: regulation, dysregulation and contributions to chronic kidney disease, Biochim. Biophys. Acta Mol. Basis Dis 2019 (1865) 1041–1066.

[25]. Hisatsune C, Kuroda Y, Nakamura K, Inoue T, Nakamura T, Michikawa T, Mizutani A, Mikoshiba K, Regulation of TRPC6 channel activity by tyrosine phosphorylation, J. Biol. Chem 279 (2004) 18887–18894. [PubMed: 14761972]

[26]. Shi J, Geshi N, Takahashi S, Kiyonaka S, Ichikawa J, Hu Y, Mori Y, Ito Y, Inoue R, Molecular determinants for cardiovascular TRPC6 channel regulation by Ca2+/calmodulin-dependent kinase II, J. Physiol 591 (2013) 2851–2866. [PubMed: 23529130]

[27]. Bousquet SM, Monet M, Boulay G, Protein kinase C-dependent phosphorylation of transient receptor potential canonical 6 (TRPC6) on serine 448 causes channel inhibition, J. Biol. Chem 285 (2010) 40534–40543. [PubMed: 20961851]

[28]. Seo K, Rainer PP, Lee DI, Hao S, Bedja D, Birnbaumer L, Cingolani OH, Kass DA, Hyperactive adverse mechanical stress responses in dystrophic heart are coupled to transient receptor potential canonical 6 and blocked by cGMP-protein kinase G modulation, Circ. Res 114 (2014) 823–832. [PubMed: 24449818]

[29]. Montalvo RN, Doerr V, Min K, Szeto HH, Smuder AJ, Doxorubicin-induced oxidative stress differentially regulates proteolytic signaling in cardiac and skeletal muscle, Am. J. Physiol. Regul. Integr. Comp. Physiol 318 (2020) R227–R233. [PubMed: 31774307]

[30]. Salas-Ramirez KY, Bagnall C, Frias L, Abdali SA, Ahles TA, Hubbard K, Doxorubicin and cyclophosphamide induce cognitive dysfunction and activate the ERK and AKT signaling pathways, Behav. Brain Res 292 (2015) 133–141. [PubMed: 26099816]

[31]. Mohammed S, Shamseddine AA, Newcomb B, Chavez RS, Panzner TD, Lee AH, Canals D, Okeoma CM, Clarke CJ, Hannun YA, Sublethal doxorubicin promotes migration and invasion of breast cancer cells: role of Src family non-receptor tyrosine kinases, Breast Cancer Res. 23 (2021) 76. [PubMed: 34315513]

[32]. Christidi E, Branham LR, Regulated cell death pathways in doxorubicin-induced cardiotoxicity, Cell Death Dis. 12 (2021) 339. [PubMed: 33795647]

[33]. Palayoor ST, Stein JM, Hait WN, Inhibition of protein kinase C by anti neoplastic agents: implications for drug resistance, Biochem. Biophys. Res. Commun 148 (1987) 718–725. [PubMed: 3689368]

[34]. Takeuchi N, Nakamura T, Takeuchi F, Hashimoto E, Yamamura H, Inhibitory effect of mitoxantrone on activity of protein kinase C and growth of HL60 cells, J. Biochem 112 (1992) 762–767. [PubMed: 1295884]

[35]. Koka S, Das A, Zhu SG, Durrant D, Xi L, Kukreja RC, Long-acting phosphodiesterase-5 inhibitor tadalafil attenuates doxorubicin-induced cardiomyopathy without interfering with chemotherapeutic effect, J. Pharmacol. Exp. Ther 334 (2010) 1023–1030. [PubMed: 20543097]

[36]. Zhao XX, Cho H, Lee S, Woo JS, Song MY, Cheng XW, Lee KH, Kim W, BAY60-2770 attenuates doxorubicin-induced cardiotoxicity by decreased oxidative stress and enhanced autophagy, Chem. Biol. Interact 328 (2020), 109190. [PubMed: 32652078]

[37]. Winn MP, Conlon PJ, Lynn KL, Farrington MK, Creazzo T, Hawkins AF, Daskalakis N, Kwan SY, Ebersviller S, Burchette JL, Pericak-Vance MA, Howell DN, Vance JM, Rosenberg PB, A mutation in the TRPC6 cation channel causes familial focal segmental glomerulosclerosis, Science 308 (2005) 1801–1804. [PubMed: 15879175]

[38]. Reiser J, Polu KR, Moller CC, Kenlan P, Altintas MM, Wei C, Faul C, Herbert S, Villegas I, Avila-Casado C, McGee M, Sugimoto H, Brown D, Kalluri R, Mundel P, Smith PL, Clapham DE, Poliak MR, TRPC6 is a glomerular slit diaphragm-associated channel required for normal renal function, Nat. Genet 37 (2005) 739–744. [PubMed: 15924139]

[39]. Mukerji N, Damodaran TV, Winn MP, TRPC6 and FSGS: the latest TRP channelopathy, Biochim. Biophys. Acta 1772 (2007) 859–868. [PubMed: 17459670]

[40]. Schlondorff J, Del Camino D, Carrasquillo R, Lacey V, Poliak MR, TRPC6 mutations associated with focal segmental glomerulosclerosis cause constitutive activation of NFAT-dependent transcription, Am. J. Physiol. Cell Physiol 296 (2009) C558–C569. [PubMed: 19129465]

[41]. Heeringa SF, Moller CC, Du J, Yue L, Hinkes B, Chernin G, Vlangos CN, Hoyer PF, Reiser J, Hildebrandt F, A novel TRPC6 mutation that causes childhood FSGS, PLoS One 4 (2009), 7771.

[42]. Azumaya CM, Sierra-Valdez F, Cordero-Morales JF, Nakagawa T, Cryo-EM structure of the cytoplasmic domain of murine transient receptor potential cation channel subfamily C member 6(TRPC6), J. Biol. Chem 293 (2018) 10381–10391. [PubMed: 29752403]

[43]. Kalivendi SV, Konorev EA, Cunningham S, Vanamala SK, Kaji EH, Joseph J, Kalyanaraman B, Doxorubicin activates nuclear factor of activated T-lymphocytes and Fas ligand transcription: role of mitochondrial reactive oxygen species and calcium, Biochem. J 389 (2005) 527–539. [PubMed: 15799720]

[44]. Yoon JJ, Son CO, Kim HY, Han BH, Lee YJ, Lee HS, Kang DG, Betulinic acid protects DOX-triggered cardiomyocyte hypertrophy response through the GATA-4/calcineurin/NFAT pathway, Molecules 26 (2020).

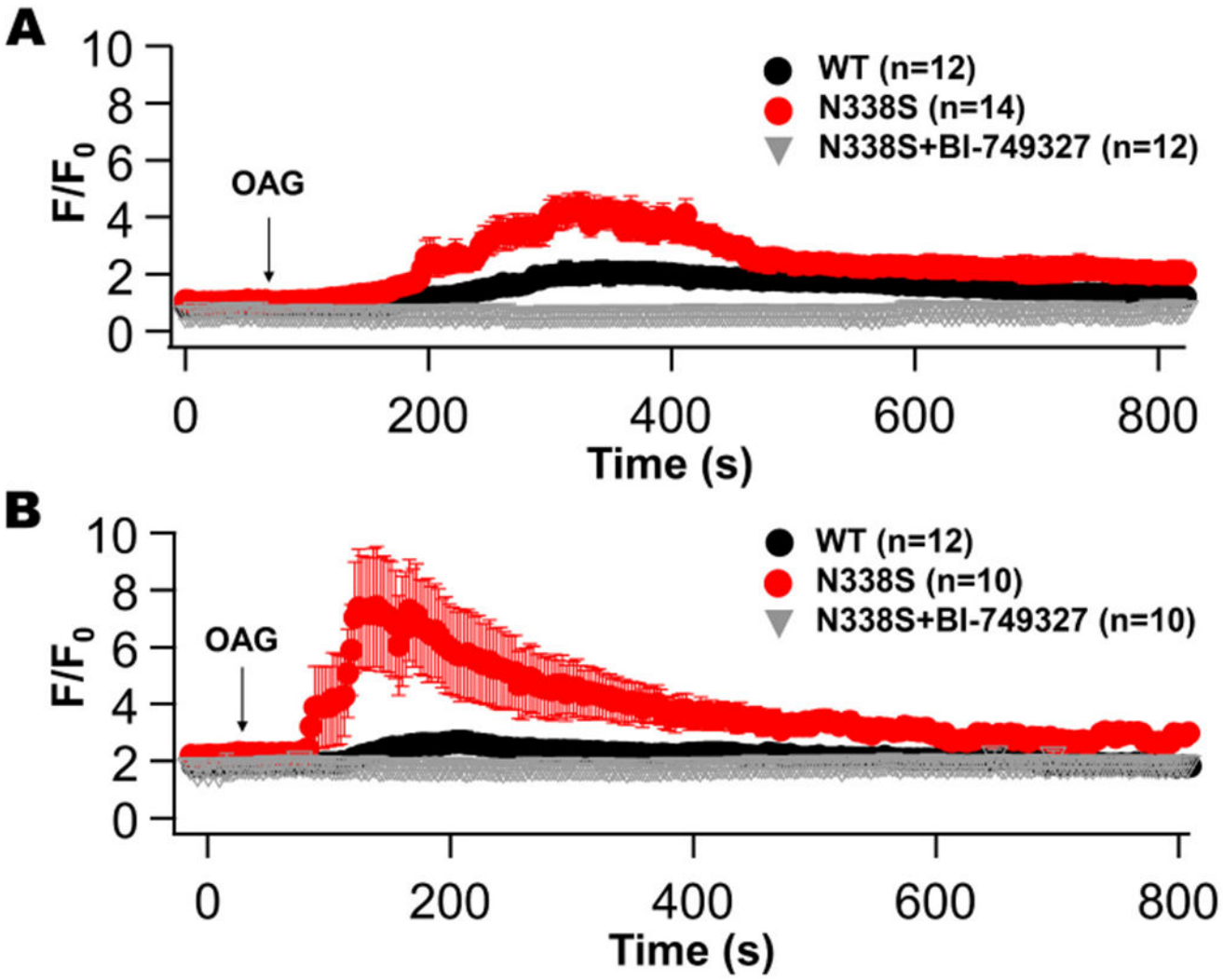

Fig. 1.

Enhanced intracellular Ca^{2+} levels in HEK293 cells expressing TRPC6 WT and N338S mutant in response to OAG and DOX treatments. A: Superfusion with OAG (50 μM) significantly increased $[Ca^{2+}]_i$ in HEK293 cells 48 h after transfection with TRPC6 N338S, compared to those with TRPC6 WT. B: The effects OAG on $[Ca^{2+}]_i$ was significantly potentiated by preincubation with DOX (0.5 μM) in TRPC6 N338S. The intracellular Ca^{2+} increase in TRPC6 WT and N338S was abolished by pre-treatment with a highly selective TRPC6 inhibitor, BI-749327 (1 μM). N = 10–14 cells from three experiments.

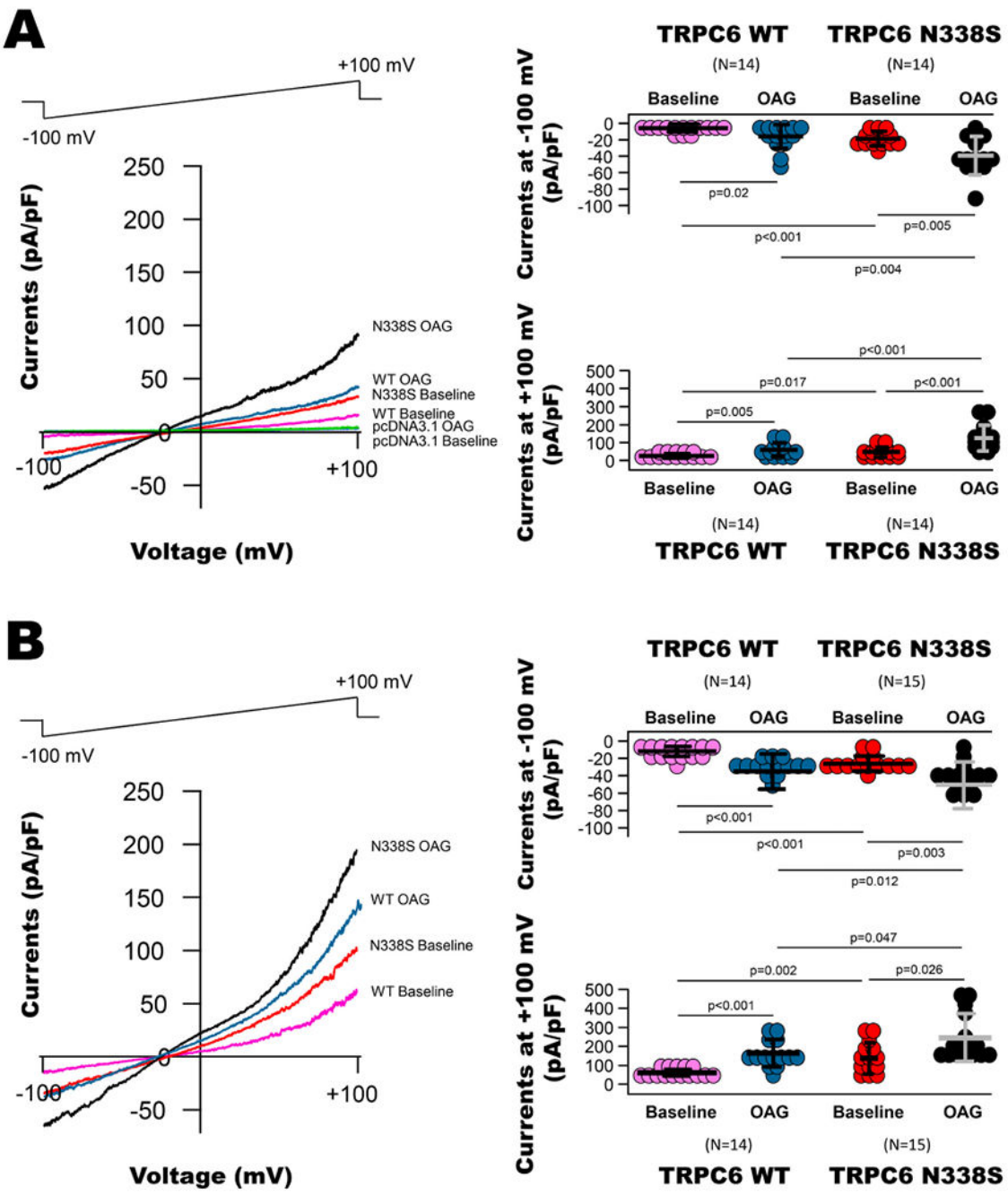

Fig. 2.

Effects DOX on OAG-mediated TRPC6 WT and N338S mutant activation in HEK293 cells. A: Whole-cell currents were elicited from HEK293 cells 48 h after transfection with TRPC6 WT and TRPC6 N338S mutant, using a voltage-ramp protocol from −100 mV to +100 mV over 100 ms at a holding potential of −60 mV. At baseline, the N338S mutant has a similar inward current density (pA/pF) at −100 mV and a slightly higher outward current density at +100 mV compared to TRPC6 WT. A 1-h incubation with OAG (50 μM) increased the inward and outward current densities of TRPC6 WT, and the OAG

effects were significantly greater in the N338S mutant. Very small currents were recorded at baseline and with OAG stimulation in cells with empty pcDNA3.1 plasmid transfection (as a transfection control). Group results with statistical significance are shown in Scatter dot plots. B: HEK293 cells were pretreated with DOX (0.5 μM) 24 h after transfection with TRPC6 WT or TRPC6 N338S. After a 48-h transfection, whole-cell currents were elicited at baseline and after a 1-h incubation with OAG (50 μM). DOX significantly enhanced the inward and outward current densities of TRPC6 N338S at baseline and markedly augmented the channel response to OAG activation, compared to those of TRPC6 WT. Group results with statistical significance are shown in Scatter dot plots.

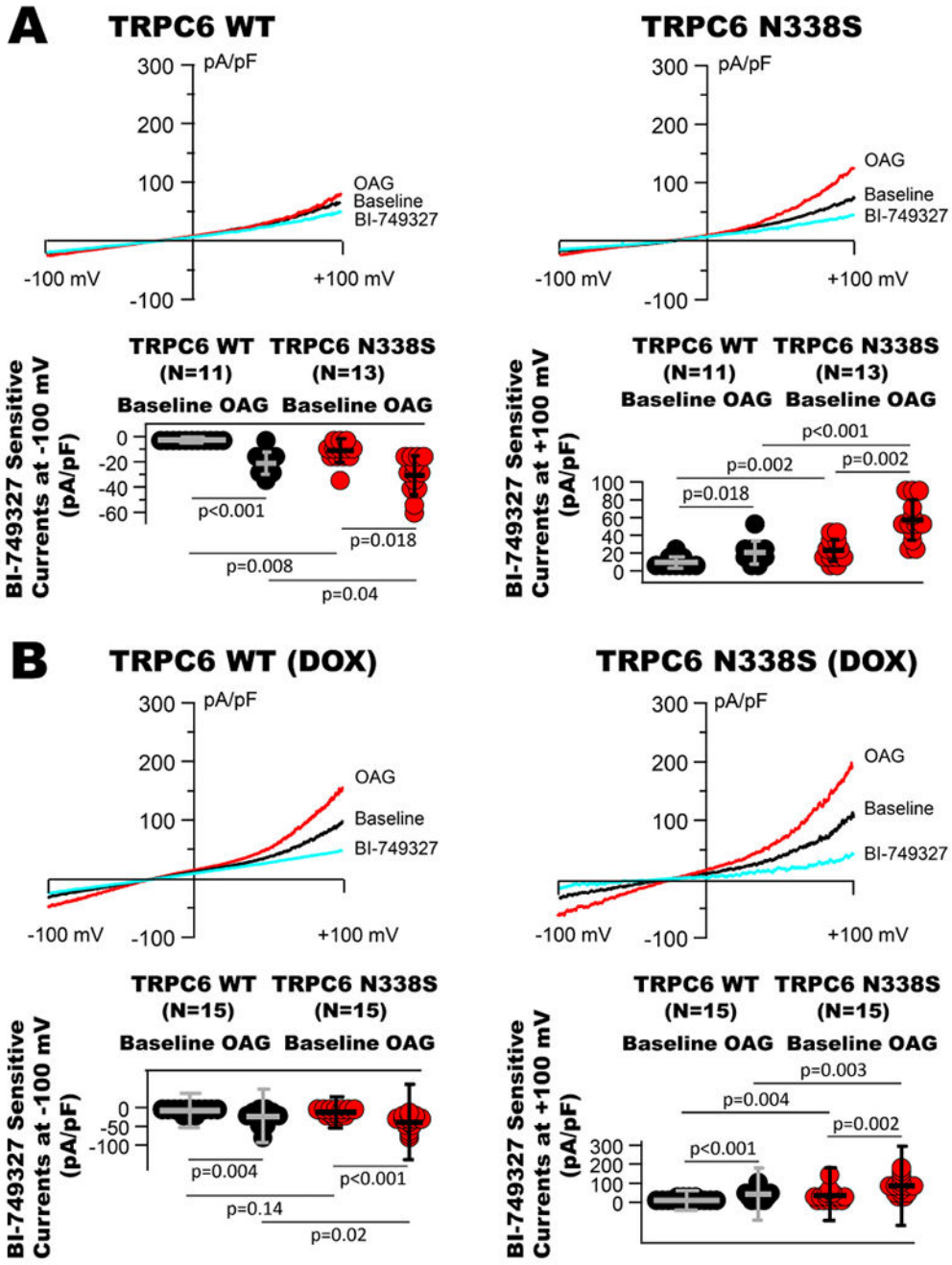

Fig. 3.

Augmentation of the OAG response in HL-1 cardiac cells expressing TRPC6 N338S in the presence of DOX. A: HL-1 cells were transiently co-transfected with TRCP6 WT or N338S cDNAs, together with GFP cDNAs. After a 48-h expression, transfected cells were identified by GFP and total cation currents were recorded from the cells at baseline and application of OAG (50 μM). At maximal activation of OAG, BI-749327 (1 μM) was superfused. The TRPC6 currents (defined as BI-749327-sensitive components) were obtained by digitally subtracting the total currents from residual currents in the presence of

BI-749327. The BI-749327-sensitive current densities were significant higher in the cells with N338S expression. B: HL-1 cells were pretreatment with DOX (0.5 μM) 24 h after transfection with TRPC6 WT or TRPC6 N338S mutant. Non-specific cation currents are shown at baseline and with application of OAG (50 μM) and BI-749327 (1 μM) 24 h after pretreatment with DOX. There is a marked increase in BI-749327-sensitive current densities at baseline and with OAG activation in the cells transfected with TRPC6 N338S, compared to the cells transfected with TRPC6 WT, as well as with cells transfected with N338S without treatment with DOX. Group data with statistical significance are shown in the Scatter dot plots.

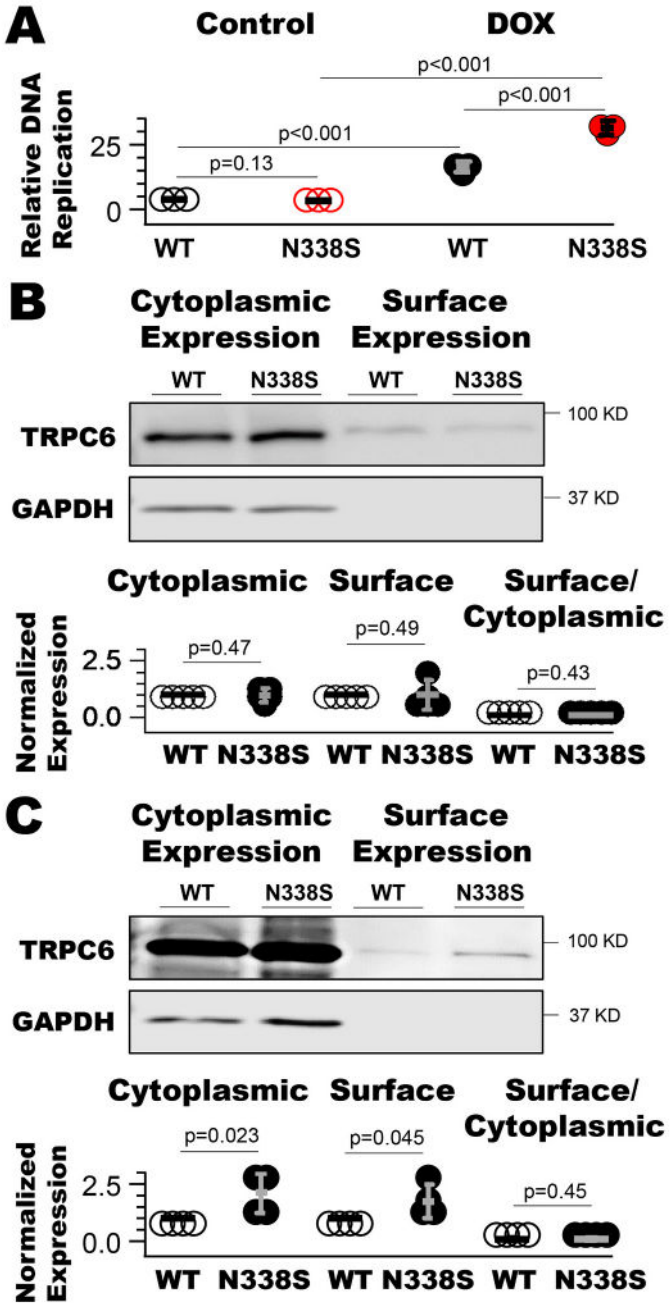

Fig. 4.

Regulation of the mRNA and protein expressions of TRPC6 WT and N338S mutant by DOX. A: Scatter dot plot with statistical analysis illustrates a 4.26- and 9.02-fold increase in the mRNA levels of TRPC6 WT and N338S mutant respectively in HEK293 cells 24 h after transfection followed by another 24 h of incubation with DOX (0.5 μM) or DMSO (vehicle control). The mRNA expression is represented by the relative cDNA replication (2^{-ct}) to a house keeping gene, *GAPDH*, n = 3 repeats. B: Surface biotinylated proteins and cytoplasmic proteins of TRPC6 WT and N338S mutant were detected in HEK293 cells

48 h after transfection in the presence of DMSO (control). Neither surface biotinylated nor cytoplasmic protein levels of TRPC6 WT and N338S mutant are significantly different, n = 5 repeats. C: A 24-h treatment with DOX (0.5 μM) significantly increases the cell surface biotinylated and cytoplasmic protein expression of TRPC6 N338S, but the ratio of surface biotinylated and cytoplasmic protein levels remains unchanged, compared to those of TRPC6 WT, n = 4 repeats. GAPDH served as cytoplasmic protein controls and loading controls.

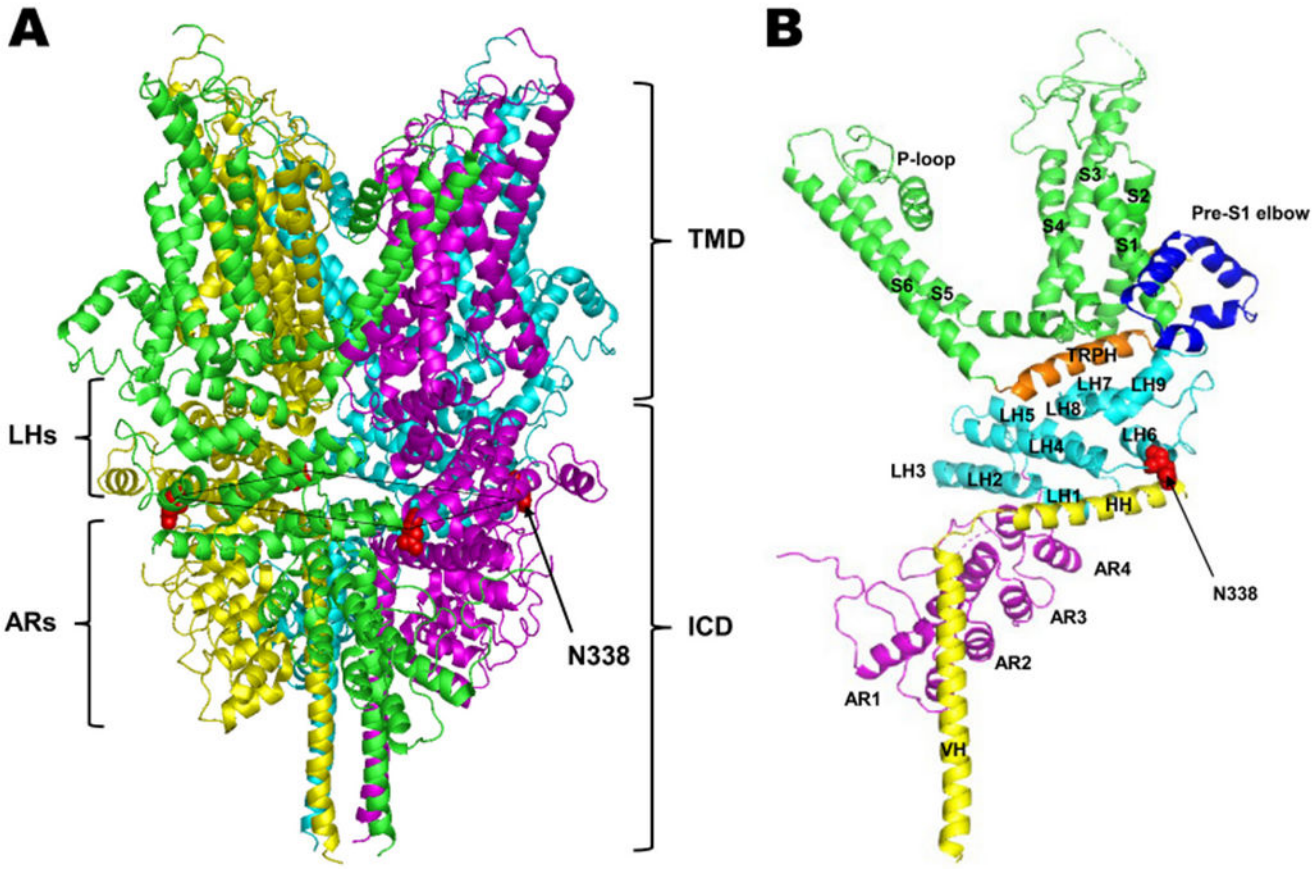

Fig. 5.

Homology model of human TRPC6 WT. A: The front view of a human TRPC6 structure generated by PyMOL software using a human TRPC6 crystallized protein (PDB ID: 6UZ8). The functional TRPC6 channel is composed of 4 homologous subunits represented by green, yellow, cyan, and magenta colors. Each subunit contains an intracellular N terminus, a pre-S1 elbow (light orange), six (S1-S6) transmembrane domains (TMD), in which S1-S4 constitute the voltage sensor domain and S5-S6 form the ion-conducting pore domain with an intervening pore helix, followed by a highly conserved transient receptor potential helix (TRPH), a TRP reentrant segment and then the cytoplasmic C terminus. The four P-loops from each TRPC6 subunit are critical for channel Ca^{2+} permeability. The pre-S1 and the TRP reentrant segment are halfway embedded in the membrane. The intracellular cytoplasmic domain (ICD) is relatively large, containing four ankyrin repeats (ARs) followed by nine linker helices (LHs) at the N-terminus, while the cytoplasmic C-terminus is smaller, composed of a vertical helix (VH) and a horizontal helix (HH) that connects to the VH via a short linker with a 90° turn and inserts into the cavities between the ARs and HHs of two adjacent subunits, anti-parallel to the TRPH. Both N- and C-termini contribute to the tetrameric assembly of TRPC6 channels. The ARs and LHs constitute the major architecture of the intracellular cytoplasmic domains of TRPC6 channels and the last three (LH7-LH9) pack against the TRPH, forming an inverted dome-like chamber that provides major contact interfaces between the cytoplasmic and transmembrane domains of TRPC6

channel. The N338 residues are indicated by red colors in each subunit. B: Detail structure of a single human TRPC6 subunit. Single TRPC6 subunit contains several domains (from the cytoplasmic N-terminus): four ankyrin repeats (AR1–4, residues 96–243, magenta), nine linker helices (LH1–9, residues 256–393, cyan), the pre-S1 elbow (residues 396–438, blue), six transmembrane segments with a pore-loop (S1-S6, residues 439–733 including the pore helix: residues 671–683, green), the TRP helix (TRPH) with the TRP reentrant segment (residues 737–751, brown), the horizontal helix (HH, residues 767–875, yellow), the horizontal helix-vertical helix linker (residues 876–879, yellow), and the vertical helix (VH, residues 880–921, yellow). (For interpretation of the references to colour in this figure legend, the reader is referred to the web version of this article.)

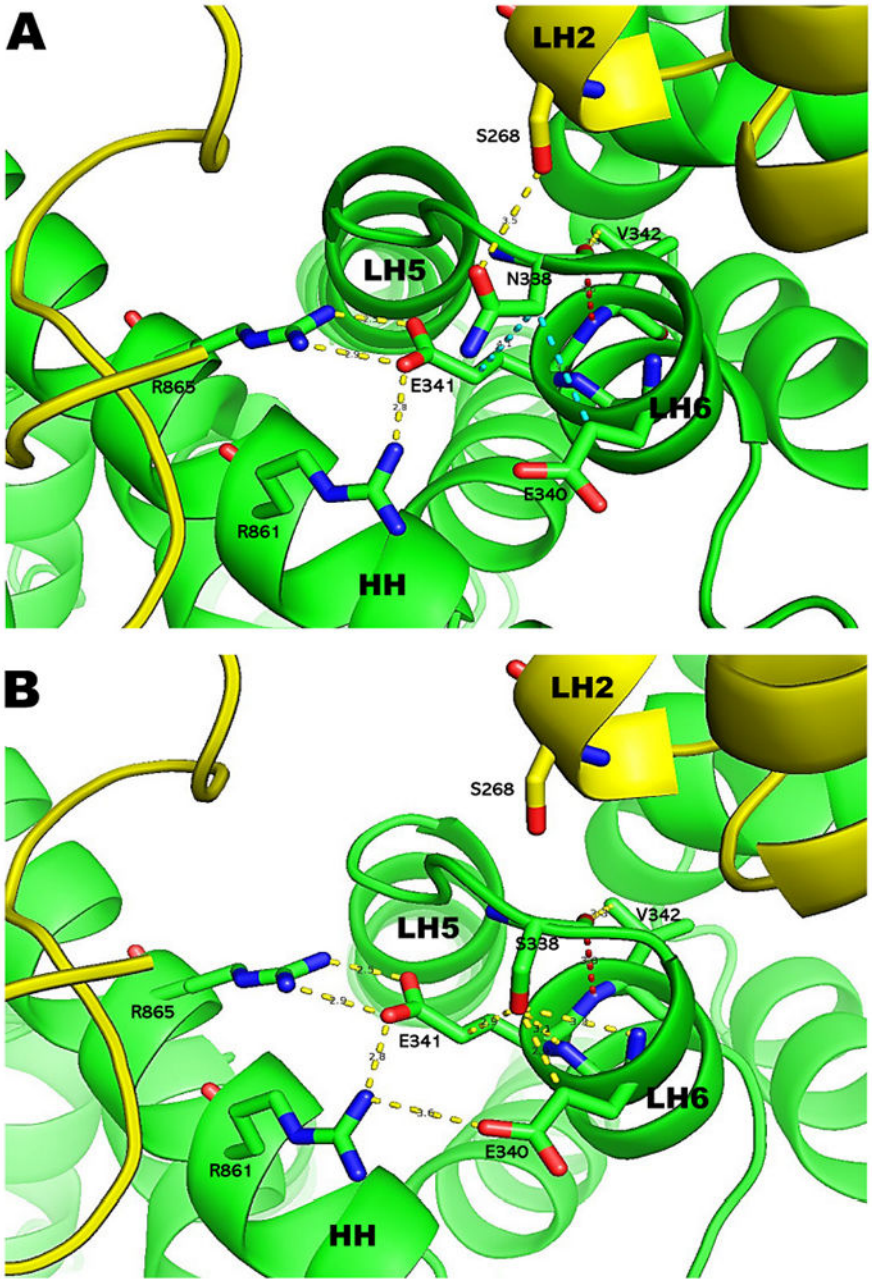

Fig. 6.

Close-up view of the conformational changes in TRPC6 N338S structure. A: Close-up view of the N338 residue in two adjacent subunits of human TRPC6 WT. The N338 residue is located at the beginning of LH6 domain, and it is in proximity with the distal end (N-terminus) of HH domain in the same subunit (green). The N338 interacts with an adjacent residue E340 via a hydrophobic interaction (3.9 Å), with E341 via a hydrophobic interaction (4.1 Å) and a polar bond (3.1 Å), and with V342 via a hydrogen bond (3.6 Å) and a polar bond (3.3 Å). The E341 forms electrostatic interactions with R861 (2.8 Å) and R865 (2.1

Å and 2.9 Å) in HH of the same subunit (green). In addition, the N338 connects to S268 via a hydrophobic interaction in LH2 of an adjacent subunit (yellow). B: Unlike N338, the S338 mutant connects to E340 via two polar bonds (2.9 Å, and 3.3 Å), to E341 via two polar bonds (2.9 Å and 3.1 Å), and to V342 via a polar bond (3.3 Å) and a hydrogen bond (3.6 Å) within the same subunit (green) and interrupts the connection with S268 in LH2 of an adjacent subunit (yellow). The N338S mutation does not change the electrostatic interactions between E340 and R861 (2.8 Å) and R865 (2.5 Å and 2.9 Å) but converts an additional polar bond (3.6 Å) between E340 and R681 in HH of the same subunit. The colored dashed lines represent h9ydrophobic interactions (cyan), polar bonds (yellow) and hydrogen bond (red). (For interpretation of the references to colour in this figure legend, the reader is referred to the web version of this article.)

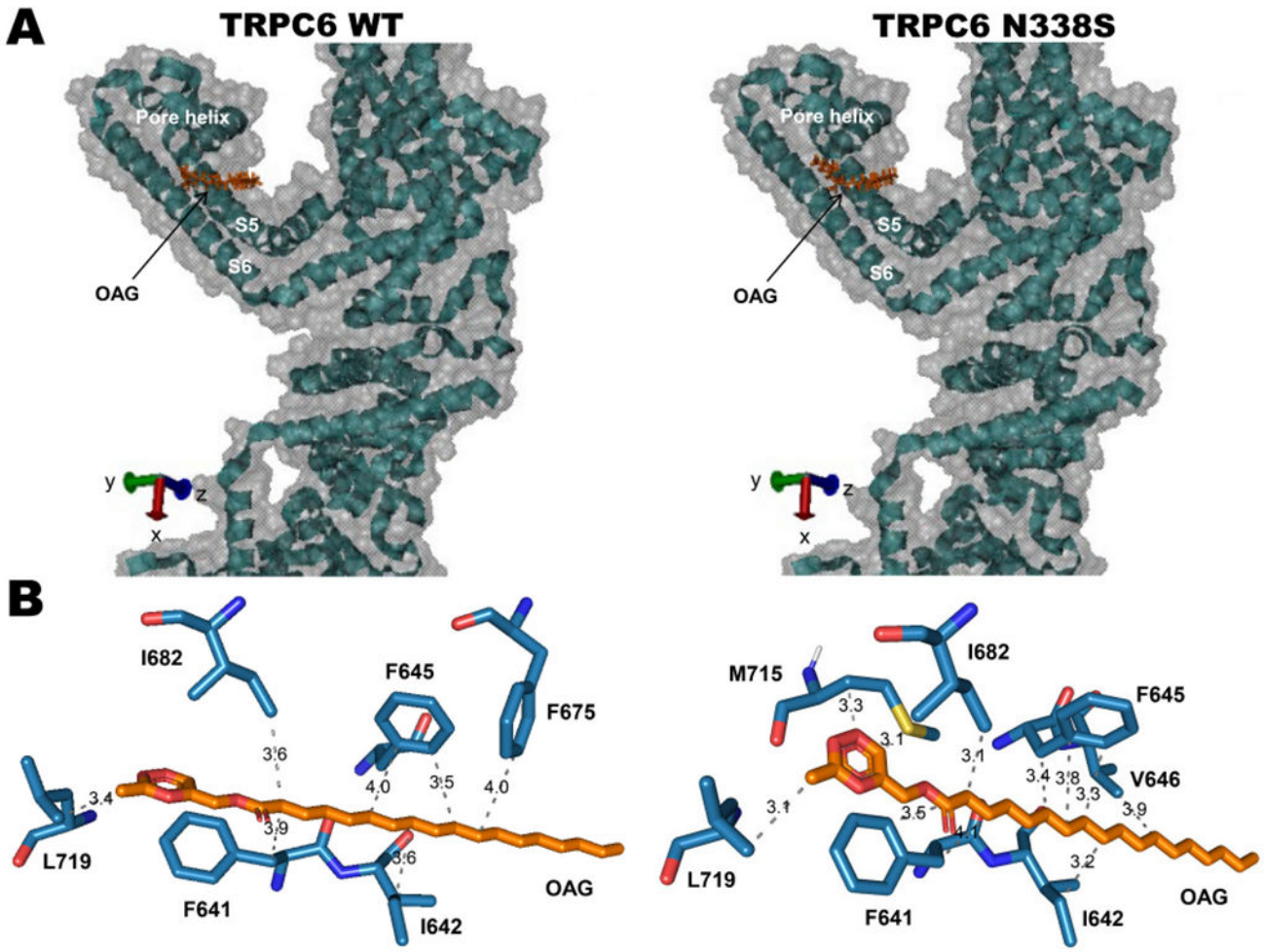

Fig. 7.

Docking of OAG to the region of TRPC6 WT and N338S mutant structures. A: OAG binds to the groove constituted by the pore helix, S5 and S6 domains of TRPC6 WT (left) and N338S mutant (right). B: The molecular binding details of OAG on TRPC6 WT (left) and N338S mutant (right). In TRPC6 WT, the oleoyl glycerol chain and the acetyloxy group of OAG form polar interactions with F641, I642, and F645 in S5, with F675 and I682 in the pore helix, and with L719 in S6, respectively. For TRPC6 N338S, similar interactions but shortened distances are taken place between the N338S and OAG, at which the interaction of OAG with F675 in the pore helix of TRPC6 WT is replaced by V646 in the S5 of N338S, and an additional M715 in the S6 of N338S forms two new interactions with the acetyloxy group of OAG via a polar bond and a hydrogen bond.

Table 1

Docking simulation of OAG.

Protein	Total number of seeds	Cluster RMSD (Å)	Binding energy (kcal/M)	Dissociation rate constant, Kd (pM)	Number of hydrogen bonds	Amino acids involved ligand-protein interaction
WT	10,016	0	−13.09	252.65	0	F641, I642, F645, F675[a], I682, L719
N338S	9613	0	−13.97	77.71	1	F641, I642, F645, V646[a], I682, M715[a], L719

[a]The difference of amino acids involved in the interaction of OAG with TRPC6 WT and TRPC6 N338S mutant.

Biochim Biophys Acta Mol Basis Dis. Author manuscript; available in PMC 2024 February 10.